Li-ion Battery Recycling by Energy-Efficient, High-Throughput Li_2SO_4 Salt Splitting in a Diaphragm Flow Cell

Jason W. Misleh[†], *J. Gage Wright*[†], *Benjamin P. Charnay*[†], *Matthew W. Kanan*[†]*

[†] Department of Chemistry, Stanford University, Stanford, California 94305, United States

*Corresponding author may be emailed at: mkanan@stanford.edu

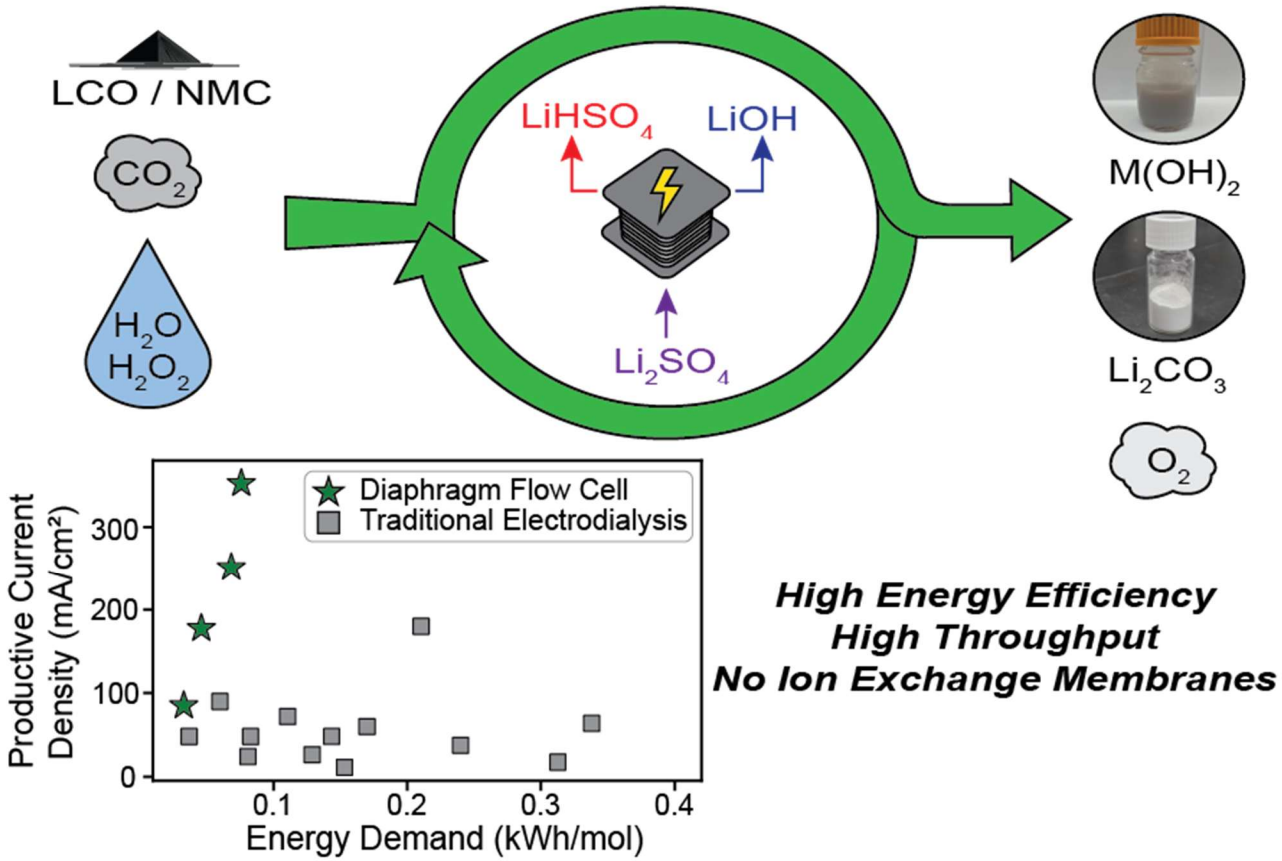

Abstract

Rapidly growing demand for lithium-ion batteries (LIBs) necessitates a significant expansion of LIB recycling to ensure adequate supply and avoid waste buildup. Traditional hydrometallurgical LIB recycling processes use super-stoichiometric quantities of acid and base and generate large volumes of salt waste which pose an environmental burden. Electrochemical regeneration of acid and base from salt offers a zero-waste alternative but faces challenges with respect to throughput and energy consumption, with current densities typically limited to ≤ 100 mA/cm^2 and energy demands > 0.10 kWh/mol. These limitations stem from a reliance on ion exchange membranes (IEMs), which lead to high cell resistance. This study reports a hydrometallurgical process to recycle lithium cobalt oxide (LCO) and lithium nickel manganese cobalt oxide (NMC) cathodes using acid and base electrochemically generated from a Li_2SO_4 electrolyte. The electrochemical cell used contains no IEMs, enabling excellent energy efficiency between 0.033 - 0.097 kWh/mol at current densities up to 500 mA/cm^2 and imparting a robust tolerance for impurities that typically foul IEMs. The produced acid and base are found to be competent for etching and recovering > 90% of the valuable metals from LIBs at industrially relevant pulp densities up to 66 g/L, and are readily regenerated from the salt solution left at the end of the metal recovery process.

Keywords: Salt Splitting, Li-ion Battery Recycling, Hydrometallurgy, Electrolyzer Engineering, pH Swing

The global demand for LIBs has grown from 158 GWh/yr in 2020 to more than 1 TWh/yr in 2024 [1, 2]. This growth was largely fueled by the massive demand for electric vehicles (EVs), with a 25% increase in EV battery demand in 2024 to 950 GWh [1–3]. The rapid expansion of the LIB market means that in the near future the flow of end-of-life batteries will also dramatically increase, with reports estimating between 400 and 1500 GWh of spent batteries and production scrap generated per year by 2030 [4, 5]. Recycling spent batteries, particularly the critical mineral-containing cathodes, is necessary both to avoid toxic waste buildup and prevent gross inefficiencies when sourcing the materials for new batteries. One ton of battery grade Li can come from 750 tons of brine, 250 tons of spodumene ore, or just 28 tons of spent LIBs. For Co, 15 tons of spent LIBs contain the same amount of Co as 300 tons of ore [6]. Capitalizing on this highly concentrated source of critical minerals has become a priority for governments worldwide to improve their energy security. Annex XII of the European Battery Regulation, for instance, has mandated a 95% recycling rate for Co, Ni, and Cu and 80% for Li by the end of 2031 across the European Union [7]. Cathodes based on the $LiNi_xMn_yCo_zO_2$ (NMC) and $LiCoO_2$ (LCO) chemistries represent a major portion of LIBs globally, especially in Europe and the United States where NMC and LCO cathodes comprise >

60% of the LIB supply [8–10]. In addition, they contain far more valuable metals than the main competing battery chemistry $LiFePO_4$, making them priority targets for recycling.

NMC and LCO cathodes are recycled through either a pyrometallurgical or hydrometallurgical route, with hydrometallurgy considered more economical and efficient for obtaining high yields of high purity products [11]. In hydrometallurgy, strong acids and reducing reagents are employed to dissolve the valuable metal ions in the cathode active material (CAM), and bases such as NaOH and Na_2CO_3 are ultimately used to precipitate the transition metals and lithium, respectively [12]. While the hydrometallurgical route has several advantages including high material recovery and low energy consumption, the process also suffers from waste accumulation as a result of stoichiometric consumption of acid and base [11–14]. An industry report estimated that for every metric ton of battery grade precursor produced from hydrometallurgical recycling processes, 1.5 metric tons of Na_2SO_4 salt waste are co-generated [15]. In addition, the use of some mineral acids such as HCl and HNO_3 is associated with toxic gas emissions during the leaching step [16, 17]. Furthermore, the continuous introduction of alkaline Na^+ salts leads to purity concerns for the recovered Li^+ as Na^+ has a strong tendency to co-precipitate with Li^+ salts, ultimately requiring purification steps that will generate even more salt waste [18, 19].

The problems arising from the stoichiometric use of inorganic acids and bases have spurred research into alternative methods to reduce waste product toxicity or prevent waste accumulation. The use of environmentally innocuous organic acids (e.g. citric, formic, acetic, malic) to replace inorganic acids has been extensively investigated [20–26]. However, despite their low toxicity and moderate efficacy for leaching CAM, organic acids are far more costly and energy intensive to produce, and may have a higher emissions footprint than inorganic acids [27–31]. Other proposals aim to prevent the generation of waste altogether by using the leftover salts to regenerate acid and base, which may be fed back into the hydrometallurgical process [32–41]. These approaches utilize ion exchange membranes (IEMs) and bipolar membranes (BPMs) in electrodialysis cells to generate acid and base, typically H_2SO_4 and LiOH. While these proposed processes do reduce or completely eliminate salt waste, the electrodialysis cells suffer from high energy demand due to the significant resistivity of the IEMs. Large resistance penalties and a loss of selectivity at high current densities also limit the current densities IEMs can pass to ~100 mA/cm^2, limiting the throughput of the electrodialysis approach. Finally, IEMs and BPMs are expensive and vulnerable to degradation, with cation exchange membranes being particularly susceptible to degradative scaling in the presence of even small concentrations of multivalent cations [42–46].

Here we present a CAM recycling scheme to regenerate acid and base from the leftover salt using an electrochemical diaphragm flow cell (DFC) that contains no IEMs. We demonstrate the ability of the DFC to output a wide range of concentrated acid and base streams with a Li_2SO_4 electrolyte, the competency of the output acid for digestion of

CAM, and the recovery of all valuable transition metals and Li^+. By avoiding IEMs we eliminate the high resistance barriers to ion transport, enabling the DFC to operate with competitive energy efficiency (< 0.10 kWh/mol) at current densities from 100-500 mA/cm^2, several times greater than those in analogous electrodialysis systems. The removal of the sensitive charged polymers in IEMs further allows us to recycle our electrolyte without any pretreatment. The proposed process may be an economically viable strategy for recycling NMC and LCO batteries while avoiding continuous reagent inputs and waste generation.

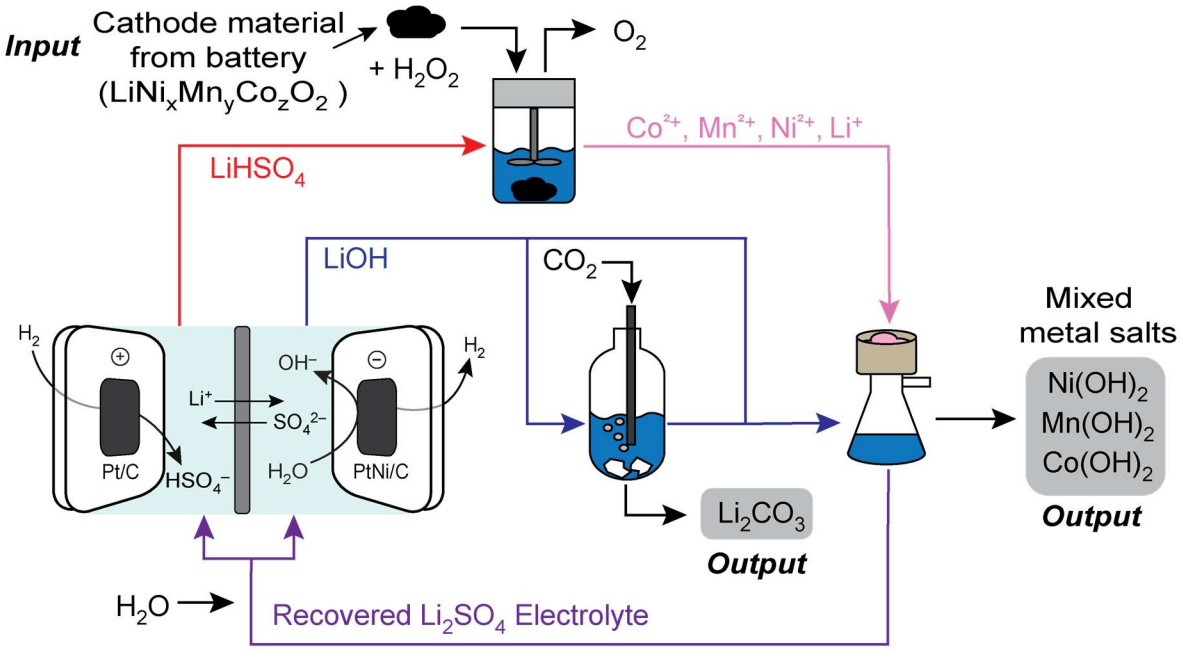

Fig. 1 Overview of LIB recycling process

The process, depicted in Fig. 1, consists of four steps: (i) generation of $LiHSO_4$ acid and LiOH base from a Li_2SO_4 electrolyte, (ii) chemical leaching of transition metals and Li^+ from CAMs using the acid stream, (iii) recovery of Li^+ as Li_2CO_3 by carbonating 1/3 of the base stream, and (iv) precipitation of transition metal hydroxides using the remaining 2/3 of the base stream. The overall reaction is represented by eq. 1, with constituent reactions described in Note S1:

$$2LiNi_xMn_yCo_zO_2 + H_2O + CO_2 + H_2O_2 \rightarrow 2x\,Ni(OH)_2 + 2y\,Mn(OH)_2 + 2z\,Co(OH)_2 + Li_2CO_3 + O_2 \qquad (1)$$

$$(x + y + z = 1)$$

Generation of acid and base streams

The electrochemical cell is a diaphragm flow cell (DFC) where a high concentration of supporting electrolyte outcompetes the transport of acid and base, enabling the output of concentrated acid and base streams [47, 48]. The cathode performs the hydrogen

evolution reaction and the anode performs the hydrogen oxidation reaction. This hydrogen looping strategy both minimizes the thermodynamic voltage to generate acid and base and requires no external supply of reactants to operate the DFC. Furthermore, we have previously demonstrated that H_2 can be recycled with > 99.9% efficiency in a stack of DFCs [47]. The DFC contains no IEMs that are normally employed to prevent the recombination of acid and base. Instead, 2 M Li_2SO_4 supporting electrolyte outcompetes

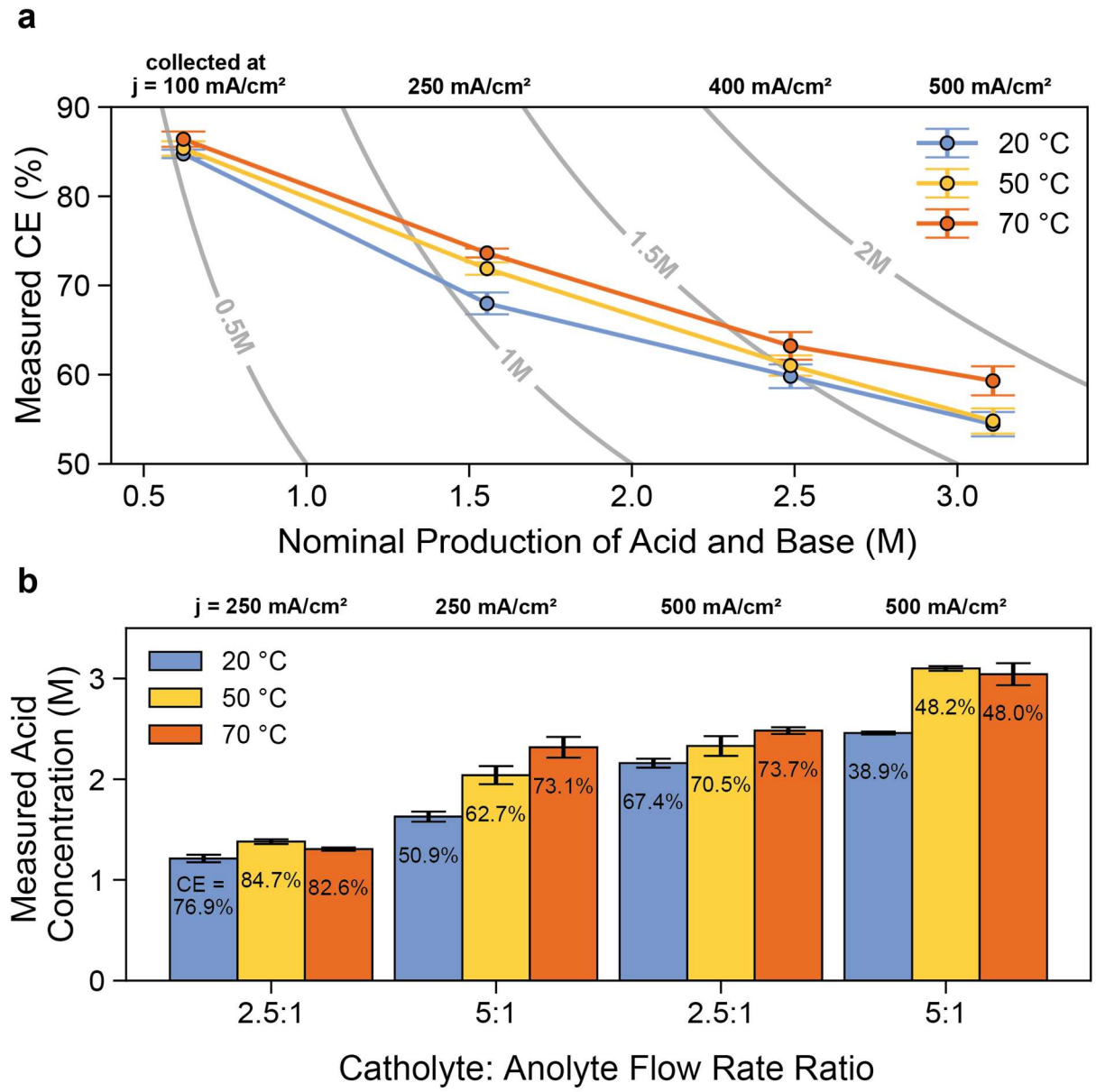

Fig. 2 (a) Current Efficiency vs. Nominal Production of acid and base. Grey tie lines represent real output concentration, assuming zero density change of the electrolyte. (b) Acid output concentration for asymmetrical catholyte : anolyte flow rates. Error bars indicate the standard error of the mean for at least n = 3 independent samples

the transport of acid and base across the non-selective diaphragm separator, decreasing the resistivity of the cell and improving the energy efficiency. In addition, SO_4^{2-} in the anolyte will equilibrate with electro-generated protons to form the negative HSO_4^- anion, which does not experience an electromigration driving force to cross the dividing diaphragm and thus further inhibits acid-base recombination.

The primary metric for measuring acid and base re-combination is current efficiency (CE), which is the mole percentage of acid and base that do not recombine to form water. A CE of 100% indicates no acid and base crossed the separator and recombined, whereas 0% indicates that all the generated acid and base was lost to recombination. Fig. 2a shows the CE at several production levels of acid and base, which are necessarily equal in concentration when the anolyte and catholyte flow rates are equal. Of particular importance for this battery recycling process is the ability to output a concentrated acid stream. Industrially relevant pulp densities of 20-100 g cathode material/L leaching solution require 0.6-3.0 M acid output to fully solubilize the valuable metals. At low concentrations near 0.5 M, the cell exhibits a CE close to 90%, indicating almost none of the acid and base cross the diaphragm. As the nominally produced concentration increases, the CE decreases. A slight increase in CE is observed when the operating temperature of the cell is raised. This benefit may be explained in part by the increased formation of LiOH contact ion pairs as the temperature is raised, owing to the endothermic association of Li^+ and OH^- [49]. The mechanism for OH^- masking also manifests as a lowering of solution pH with temperature (Fig. S1). In addition, the operating voltage of the cell is considerably lowered at higher temperatures, substantially improving the energy efficiency of acid-base generation (Fig. S2, Table S1).

With symmetric flow rates, the concentration of the acid and base plateaus at ~1.8 M, which is capable of solubilizing up to 60 g/L maximum pulp density. The precipitation of Li_2CO_3 and transition metal hydroxides, however, are both thermodynamically favored and rapid, such that high concentrations of base are unnecessary. By increasing the catholyte pump rate, the catholyte is diluted, lowering the driving force for transport of OH^- across the diaphragm. Using asymmetric flow rates combined with increased operating temperature substantially increases the CE, enabling production of > 3 M $LiHSO_4$ as shown in Fig. 2b and Table S2. The Li^+ concentration of the output acid and base was measured by ICP-OES, and by charge balance the SO_4^{2-} concentration in each compartment may be inferred (Fig. S3, Tables S3, S4). Having determined the exact composition of the acid and base outputs, we independently prepared large volumes of these solutions to study their efficacy for battery ion leaching and metal recovery.

Leaching of CAM

We used the acidic output to leach two widespread cathode chemistries, LCO and NMC 111 ($LiCo_{0.33}Ni_{0.33}Mn_{0.33}O_2$) at 50 °C. LCO is more difficult to digest in hydrometallurgical processes. In addition to acid, a continuous input of reducing agent is

needed for digestion of NMC and LCO battery chemistries. Hydrogen peroxide is chosen as a reducing agent because its only byproducts are water and oxygen, avoiding contamination of the electrolyte. We also note that the pH of the high ionic strength $LiHSO_4$ solutions output by the DFC is substantially lower than that of an ideal $LiHSO_4$ solution (Table S3), which reflects the low activity coefficient of SO_4^{2-} in solutions with large supporting cation concentrations [50, 51]. Increased acidity improves the leaching kinetics for CAM.

To be solubilized in the leaching solution, the transition metals must be in their +2 oxidation state. If no reducing agent is added, the transition metals at the surface of the

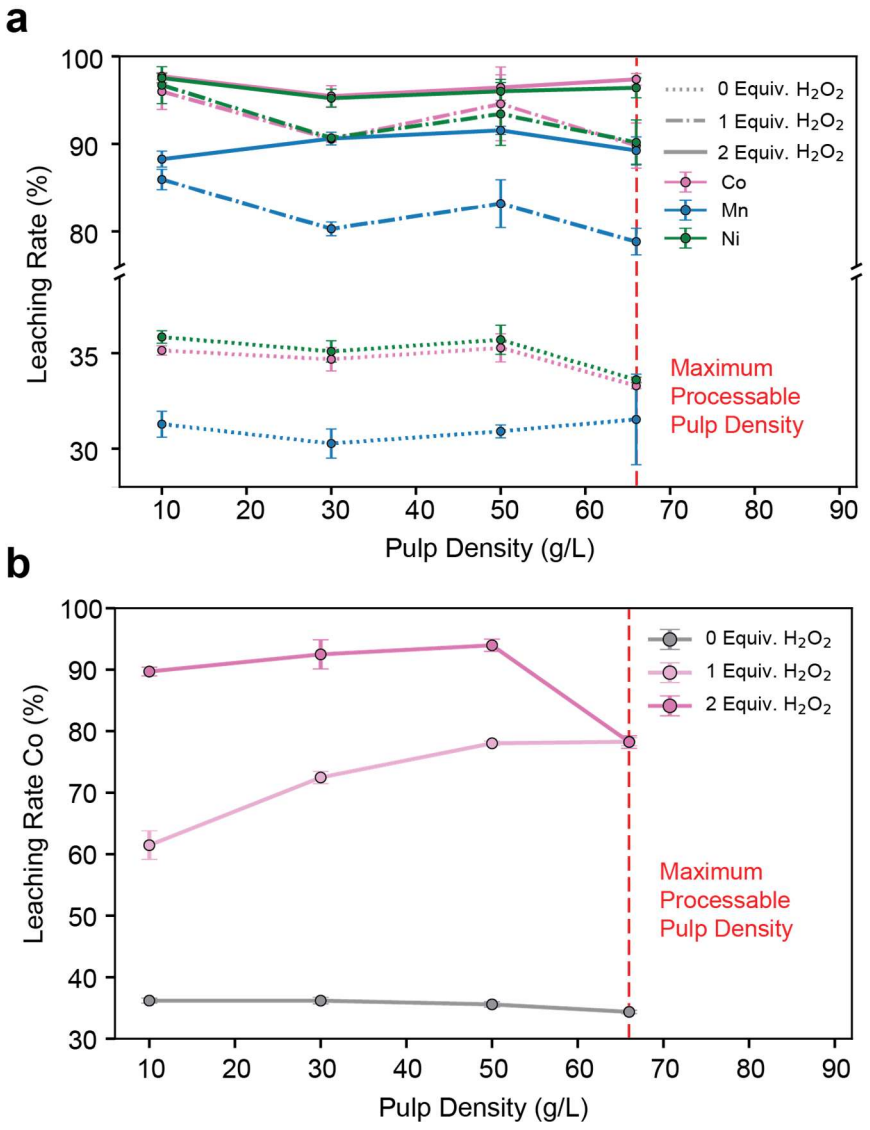

Fig. 3 Leaching rate of transition metal ions in (a) NMC 111 CAM and (b) LCO CAM using 2 M acidic solution prepared according to the measured speciation of the DFC acid output (see Table S3) at 50 °C. Error bars represent the standard error of the mean for at least n = 3 independent samples

particle will be reduced by oxygen evolution or by electron donation from the bulk, and some dissolution will occur [52, 53]. However, Fig. 3 shows that in the absence of H_2O_2, the leaching efficiency for the transition metals in both LCO and NMC remains minimal at ~30% for all pulp densities. For NMC 111, the driving force for dissolution is inhibited as delithiation progresses [52]. The addition of a single equivalent of H_2O_2 results in > 89% leaching of Ni and Co at all pulp densities. Mn oxides are more resistant towards reduction and only ~80% of Mn is leached at a pulp density of 66 g/L. We note that a single equivalent of H_2O_2 is likely insufficient for reducing all metal ions in the cathode materials despite the stoichiometry of eq. 1 as H_2O_2 spontaneously disproportionates to O_2 and H_2O to some extent when heated in the presence of metal oxides. Adding a second equivalent of H_2O_2 pushes the Ni and Co leaching rates > 95% and the Mn leaching rate to > 89% even at 66 g/L. In the case of LCO, mixed-valence cobalt oxides form around the LCO particles that water cannot quickly reduce [54]. A single equivalent of H_2O_2 again significantly improves the leaching rate for Co. A leaching rate > 90% is observed with two equivalents, except at the highest pulp density, where a higher concentration of acid is likely needed to increase the leaching rate.

Following acid leaching, any residual H_2O_2 is easily disproportionated to water and oxygen (Fig. S4) by a reusable Pt-coated disk with < 60 μg Pt/cm^2 loading on its surface [55]. As long as 2 equivalents or less of H_2O_2 are used, there will be no net dilution of the electrolyte from the acid leaching step, avoiding the need to boil off excess water (Note S2).

Recovery of Li_2CO_3

The base output of the cell, composed of LiOH and Li_2SO_4, is readily carbonated by CO_2 to yield isolable Li_2CO_3. In our closed-loop process, only a portion of the base stream is contacted with CO_2 such that the amount of Li isolated as Li_2CO_3 matches the amount of Li^+ leached from the CAM. Although Li_2CO_3 is sparingly soluble in water, this issue is sidestepped in our process by having an excess of base and a very large excess of Li^+. The solubility is further reduced by carbonating at 50 °C, as Li_2CO_3 exhibits retrograde solubility. Fig. S5 shows the pH of the alkaline lithium solution during the carbonation procedure. The precipitation is stopped when an inflection point in the pH curve is reached, indicating the solution is fully carbonated. On filtering, the white precipitate is found to have a significant Li_2SO_4 content, which is easily removed by washing 3x with a small amount of boiling water, yielding phase pure Li_2CO_3 as shown in Fig. 4a. The purity of the product was determined by potentiometric titration of the carbonate with HCl and found to have an average purity of 99.9% by mass, surpassing the battery grade purity requirement of 99.5% (Fig. S6).

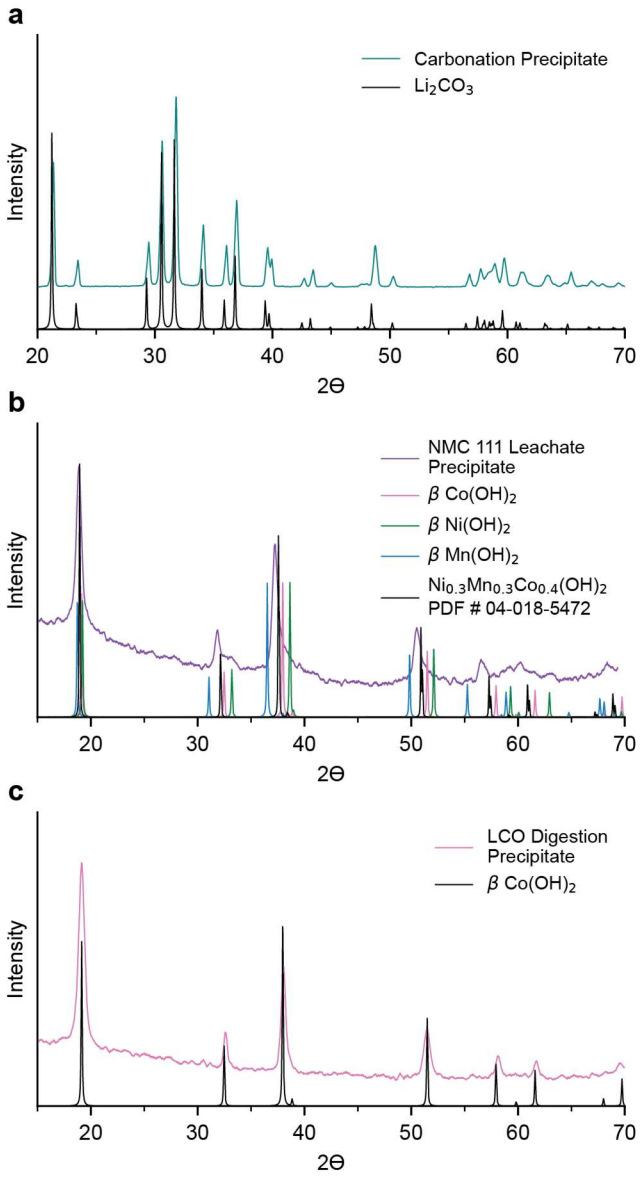

Fig. 4 (a) XRD pattern of washed Li precipitate from carbonating the base stream. (b) XRD pattern of precipitated product from the NMC 111 leachate. (c) XRD pattern of precipitated product from the LCO leachate

Recovery of Transition Metal Hydroxides

In the final step, the leachate containing the solubilized transition metals is contacted with the remaining base under N_2 and transition metal hydroxide (TMH) solids are recovered. For the NMC 111 leachate, a solid blue precipitate is formed immediately on contact that transitions to a light purple (Fig. S7), which is indicative of the transformation of an α-$M(OH)_2$ phase to β-$M(OH)_2$. The precipitate is readily filtered and rapidly turns brown in the presence of air. The XRD pattern of the precipitated material contains none of the pure TMH peaks, instead displaying a set of peaks that consistently

reside in between the pure materials (Fig. 4b). The peaks indicate a homogeneous distribution of metal cations in the blended hydroxide phase $Ni_xMn_yCo_z(OH)_2$ [56, 57]. Peak shoulders at 33 ° and 38 ° correspond to partial oxidation of the hydroxide phase to an oxy-hydroxide phase by oxygen in the air [56]. Elemental analysis of the solid product by ICP-OES confirmed the stoichiometric ratio of the transition metals matches that of the leachate (Table S5). When accounting for Li^+ and SO_4^{2-} impurities, the material is found to be at least 99.1% pure by mass (Table S5). This material can be used to directly manufacture new NMC cathodes by calcining with LiOH or Li_2CO_3 [57, 58]. When doing the same process with the LCO leachate, once again a solid blue precipitate forms that rapidly transitions to pink, phase-pure β-$Co(OH)_2$ with no apparent oxidation (Fig. 4c). Furthermore, the material is found to be 99.7% pure by mass (Table S6). Major impurities due to Fe, Cu, and Al present in black mass may be removed in the acidic pH range of 2-5 to avoid contamination of the output TMH phase [59, 60]. ICP-OES analysis of the regenerated electrolyte contains less than 1 ppm of all transition metal ions, indicating full recovery of the transition metals (Table S7).

Reuse of the Electrolyte and Energy Analysis

At the end of our process, the Li_2SO_4 electrolyte is fully regenerated and ready to be cycled back into the DFC without any pretreatment. Fig. 5a shows voltage stability traces of the DFC at several current densities using regenerated electrolyte. Every 5 hours, the current is reversed for 2 min (99.3% duty cycle) to temporarily acidify the base compartment, which we have previously found is important for maintaining anode performance and dissolving any solid hydroxides on the cathode [47, 48]. The voltage remains stable at several current densities, illustrating the robustness of the DFC's simple design. Slight improvements in cell voltage observed after pump refills are attributed to the liberation of small bubbles that collect on the internal mesh during DFC operation (Figure S8). Our electrochemical system further exhibits superior energy efficiency compared to analogous IEM-bearing electrochemical systems producing acid and base from salt splitting with a Li_2SO_4 electrolyte, as shown in Fig. 5b. Here we compare energy demand per mol of acid and base, calculated based on operating voltage and CE, vs. productive current density (j_{prod}, the operational current density multiplied by CE). At j_{prod} = 90 mA/cm^2, near the higher end of typical j_{prod} for IEM-bearing systems, the DFC outputs 0.53 M acid with an energy demand of just 0.033 kWh/mol. Even when producing 3.1 M acid at j_{prod} = 240 mA/cm^2, the DFC's energy demand remains competitive at 0.097 kWh/mol. These benefits are realized because competitive ion transport across a nonselective diaphragm avoids the inherent resistivity of IEMs present in all of the compared electrochemical systems, instead increasing the conductivity of the cell and thus lowering the operating voltage. Furthermore, the highly concentrated, proton-masking electrolyte forces spectator ions to carry a majority of the charge, ensuring a high output concentration of acid and base can still be achieved despite the loss of

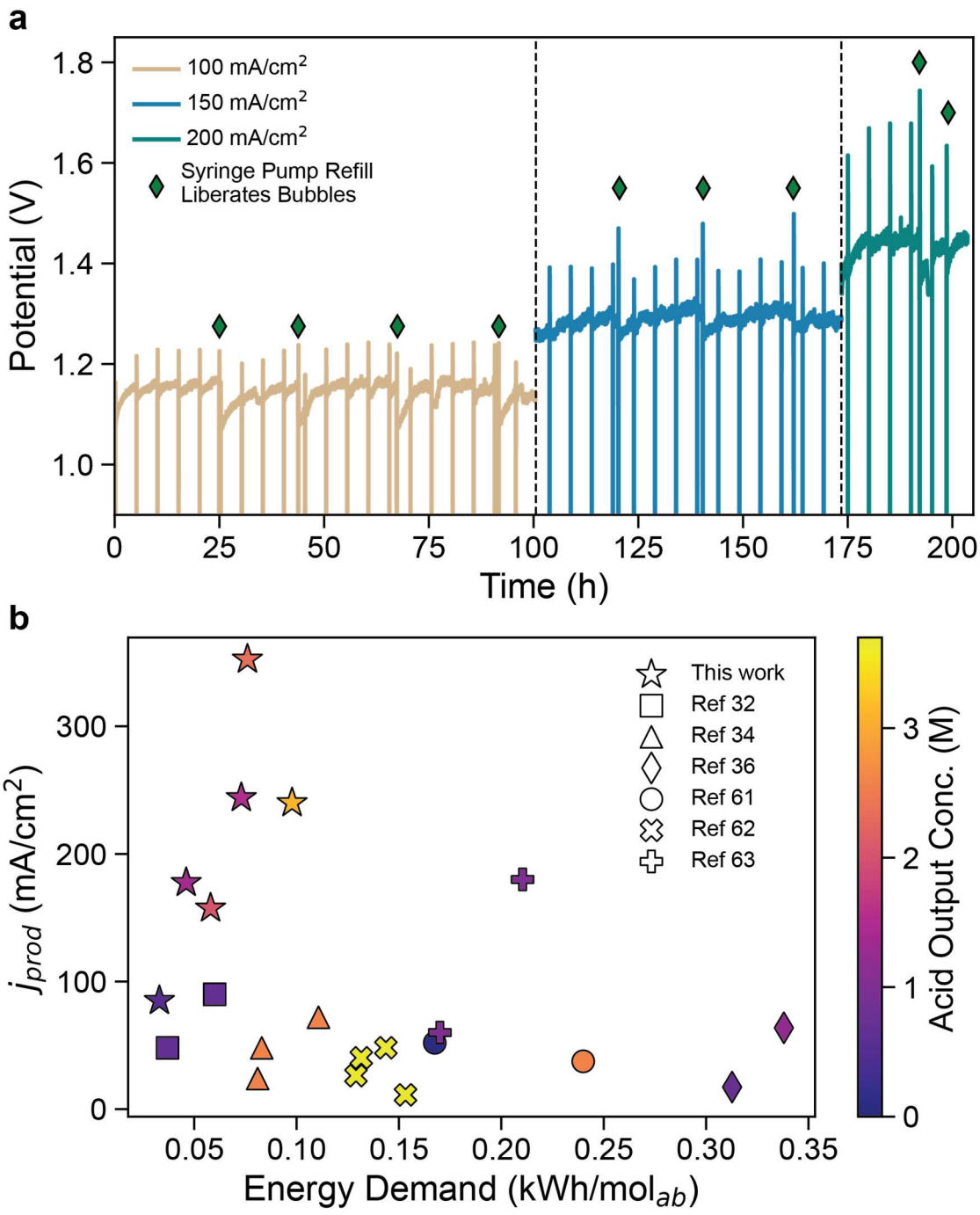

Fig. 5 (a) Voltage stability trace at several current densities using electrolyte regenerated after CAM processing. The cell was rebuilt at the dashed lines. Diamonds indicate brief pauses to refill the syringe pumps, which also liberated some small bubbles in the electrolyzer. (b) Energy demand per mol of acid and base vs. productive current density for electrochemical production of acid and base from Li_2SO_4 electrolyte. A complete tabulation of the membrane types, configuration, operating voltage, and CE of the compared salt splitting systems may be found in Table S8 [32, 34, 36, 61–63]

selectivity. Overall, our results show that foregoing selective ion transport in favor of competitive ion transport can achieve exceptional gains in energy efficiency for electrochemical acid-base production. Table S9 shows that this strategy can significantly drive down input costs for hydrometallurgical recycling processes.

Our results thus far demonstrate significant potential for a low-energy battery recycling process enabled by the DFC, but several technical barriers remain to addressed in future works. Though excellent performance metrics have been demonstrated in the DFC at the 1 cm^2 scale, multiple challenges in industrial electrochemical systems including pressure drop, gas management, and liquid flow behavior only become manifest in larger device sizes. Thus, scale-up is a priority for ensuring the DFC's advantages will replicate when translated to an industrially relevant form factor. Beyond the NMC and LCO chemistries, $LiFePO_4$ occupies an increasingly large share of the battery market. The limited value of the elements in $LiFePO_4$ batteries presents a challenge to the economics of battery recycling that a low cost, low waste recycling process using the DFC may be able to overcome, and recycling this material will be the subject of a future work.

In summary, we have developed a low-energy electrochemical method to recycle NMC and LCO cathode materials while generating zero waste. Acid and base outputs from the electrochemical cell that are efficacious in the recycling process are generated at productive current densities of hundreds of mA/cm^2, overcoming a key limitation with previous systems containing IEMs. Our process recovers > 90% of the valuable metals at industrially relevant processing pulp densities. The outputs are battery grade Li_2CO_3 and a blended mix of transition metal hydroxides that may be used to synthesize new cathode active material. Our future work will aim to scale the DFC, synthesize new state-of-the-art battery material from our recycled outputs, and extend our process to $LiFePO_4$ batteries.

Methods

Chemicals

All chemicals were used as received without further purification. Li_2SO_4 (≥ 99.5%, Sigma Aldrich), $LiCoO_2$ (≥ 99.8%, Sigma Aldrich), H_2O_2 (30 wt% in water, Sigma Aldrich), LiOH (≥99.9%, Sigma Aldrich). Li_2CO_3 (≥99%, Sigma Aldrich). $LiNi_{0.33}Mn_{0.33}Co_{0.33}O_2$ (NMC 111) was purchased from MSE supplies (≥ 99%, 3μm powder), and was determined by elemental analysis (via ICP-OES) to have the stoichiometry $LiNi_{0.35}Mn_{0.30}Co_{0.35}O_2$. This is within the manufacturer's specified composition range. Deionized water (resistivity > 18 MΩ·cm) was used to prepare all solutions.

Characterization

XRD patterns were collected with a PANalytical Empyrean diffractometer using a GaliPIX^{3D} detector and a Cu x-ray source (1.54 Å).

ICP-OES Analysis for the determination of Li, Co, Ni, and Mn concentrations were carried out on a Thermo ICAP 6300 Duo View Spectrometer with a Solid State CID Detector for multi element analysis. Observation wavelengths were 221.6 and 231.6 nm for Ni, 228.6 nm for Co, 257.6 for Mn, 670.7 nm for Li, and 180.7 nm for S.

Concentrations of H^+ and OH^- were primarily determined via colorimetric titration in the presence of phenolphthalein with NaOH and HCl standards, respectively. This method was initially validated by comparing results with potentiometric titrations of the same samples using a Mettler Toledo Routine Pro-ISM pH Electrode and NaOH and HCl standards. The two methods were found to be in excellent agreement (< 1% error). NaOH standard concentrations were determined by both colorimetric titration of a known quantity of potassium hydrogen phthalate (KHP) in the presence of phenolphthalein, and by potentiometric titration of a known quantity of KHP. HCl standard concentrations were determined by both colorimetric titration of a known volume of NaOH standard in the presence of phenolphthalein, and by potentiometric titration of a known quantity of Na_2CO_3 dried at 120 °C.

The pH of aqueous solutions was measured with a Mettler Toledo Routine Pro-ISM pH Electrode equipped with automatic temperature compensation. The electrode was calibrated before each use with Orion pH buffers (pH range 1.68 - 12.46).

Leaching experiments

Leaching experiments were carried out in 50 mL Falcon tubes using $LiHSO_4$ solution. The experiments used to collect the data for Fig. 3 were performed using a mock acid solution with $[H^+]$ = 2.06M (full composition specified in Table S3, solution 5). Authentic cell outputs of the same concentration were used when the electrolyte was to be re-generated, as in Fig. 5, and the leaching rates were found to be within error of the data for Fig. 3. The acid solutions were warmed to 50 °C in a heated vial block, then added to the cathode active material (CAM) along with a specific amount of H_2O_2. The solution was stirred at 500 rpm with a PTFE stirbar for 1 hour in the case of NMC 111 digestions, and 2 hours for LCO digestions. The leachate and residual solid were then separated by vacuum filtration using 0.22 µm Steriflip PVDF filters. Samples were immediately subjected to ICP-OES analysis to determine the leaching rate. H_2O_2 was then removed by dropping in a Pt coated plastic disk and leaving for several hours. It was found that a small amount of Mn solid will very slowly precipitate from the acidic leachate over a period of several days once the H_2O_2 is decomposed.

Li_2CO_3 Precipitation Experiments

Mock LiOH + Li_2SO_4 solutions with OH^- concentration equal to either 0.54 or 0.80 M (full compositions specified in table s4) were placed in a 50 mL falcon tubes and heated to 50 °C in a vial block. CO_2 gas was delivered at a rate of 50 sccm from an Alicat Mass Flow Controller to the LiOH + Li_2SO_4 solution while stirring at 500 rpm. A pH probe monitored the pH while gas was added, and the gas flow was stopped when an inflection point in the curve was reached. The solutions were then filtered with 0.22 μm MCE membrane filters from Millipore Sigma. The precipitate left behind was washed a specified number of times with boiling water to remove residual Li_2SO_4 on the surface (2 g H_2O/1 g precipitate per wash). Li_2CO_3 purity was determined via potentiometric titration with an HCl standard. Authentic cell output was used for the precipitation when the electrolyte was to be regenerated, as in Fig. 5.

$M(OH)_2$ Precipitation Experiments

After decomposing the H_2O_2 in the acidic leachate and precipitating Li_2CO_3 from the LiOH + Li_2SO_4 solution, both solutions were sparged with N_2. If any excess Li_2CO_3 was collected during the precipitation, it was added to the acidic leachate before adding the remaining LiOH-bearing solution, liberating CO_2 when the carbonate was neutralized. This step ensured the amount of Li^+ removed corresponds exactly to the Li^+ liberated during the leaching step, assuming 100% leaching of Li^+. The basic solution was then added to the acidic leachate all at once, and the container was capped. The solution was then stirred. If the leachate only contained Co^{2+}, the solution was stirred for 10 minutes at room temperature to allow the precipitant to transform to β-$Co(OH)_2$. If the leachate contained Ni^{2+}, Mn^{2+}, and Co^{2+}, the solution was instead stirred for 30 minutes at 70 °C to bring the transformation to completion. The precipitate was then filtered with 0.22 μm MCE membrane filters from Millipore Sigma in an N_2 glovebox and washed thoroughly with deionized water.

Cell Assembly

Assembly of the DFC is illustrated elsewhere [48] and briefly described here. The main hardware of the DFC consists of two Grade II Ti blocks, each with a multi-serpentine flow field for transporting H_2 gas. Cell assembly begins by placing guide rods in the anode electrolyzer block. A small square of 0.2 micron polypropylene-backed laminated PTFE filters from Sterlitech is placed over the multi-serpentine flow field of the anode block to prevent water from gathering in the flow field. A 0.50 mg/cm^2 Pt/C De Nora gas diffusion electrode (anode, 1 cm^2 active area) is placed over the filter. A 3D printed plastic plate of custom design is placed over the block + GDE and sealed with Buna-N o-rings, holding the GDE firmly in place. The opposite face of the plastic plate has channels to transport electrolyte, as well as a pocket that exposes the face of the GDE. A polypropylene woven mesh spacer, which had been made hydrophilic by treatment in a Diener Pico O_2 plasma cleaner, was placed inside the pocket. A 127

micron thick PTFE face gasket is placed over the flow plate, followed by a 381 micron thick polyurethane framing gasket. Inside the center hole of the framing gasket, Zirfon PERL UTP 500 (Agfa) was used as the diaphragm to separate the acid and base compartments. An additional PTFE face gasket is placed on top, followed by another polypropylene woven mesh spacer and another flow plate. A 0.88 mg/cm^2 PtNi/C GDE (cathode, 1 cm^2 active area) is placed in the electrode seat of the second flow plate, followed by another PTFE filter square. The cathode block and additional Buna-N o-rings complete the assembly. The entire assembly is placed in a vice between two heater blocks, and heated to 50 °C or the experimental operating temperature. Once at temperature, the vice is tightened with a torque wrench to 200 in-lbs. If the experiments were to be run at room temperature, the assembly was allowed to cool and then torqued once more to compensate for contraction of the metal heater blocks during cooling.

Measurement of Current Efficiency and Energy Demand

All electrochemical experiments were performed with a BioLogic VSP-3e Potentiostat. Assembled cells were pre-conditioned by passing a current of 25, -100, 250, -250, 500, and -500 mA for 1.5, 1.5, 1.0, 1.0, 0.5, and 0.5 minutes respectively. 2 to 3 equivalents of H_2 gas were supplied to the anode for all experiments, while the cathode received 1 to 1.5 equivalents to prevent depolarization by O_2 from air. Electrolyte was pumped into the cell from two NE-300 Just Infusion™ Syringe Pump from New Era Pump Systems. Aliquots were collected from the acid and base outlets after the cell had equilibrated for a minimum of 15 minutes at a specified current (100-500 mA/cm^2) and flow rate of 0.1 mL/min. For measurements with a 5 to 1 catholyte: anolyte flow ratio, the anolyte flow rate was 0.05 mL/min and the waiting period was instead 30 minutes. This waiting period corresponds to the syringe pumps passing > 3 full volumes of the electrolyte chambers and collection lines through the cell, and after this period the CE remained constant. Minimum collection times were determined by the current density, ranging from 30 minutes for samples collected at 100 mA/cm^2 to 8 min for samples collected at 500 mA/cm^2. The H^+/OH^- concentration was then determined by titration, with a small portion of the sample set aside for ICP-OES analysis if the Li content was to be measured. Current Efficiency (CE) was computed using:

$$CE = \frac{FC_{std}V_{std}}{t_{sample}\, j_{tot} A_{electrode}} \quad (2)$$

where F is the Faraday constant, C_{std} is the concentration of the acid/base standard, V_{std} is the volume of standard dispensed, t_{sample} is the time over which the aliquot was collected, j_{tot} is the current density, and $A_{electrode}$ is the active area of the electrode. CE was measured from both the acid and base outputs, and the average was reported. The energy demand of the cell was computed using:

$$E_{ab} = \frac{E_{cell}\, F}{CE} \quad (3)$$

where F is the Faraday constant and E_{cell} is the average voltage of the cell during the time the aliquots were collected.

Stability Experiments

An assembled cell was run for several hours with 2 M Li_2SO_4 + 0.001 M LiOH to produce acid and base streams. The acid and base streams were used to digest 30 g/L of NMC 111 material using the leaching procedure described above. Then Li_2CO_3 and $M(OH)_2$ (M = Ni, Mn, Co) were recovered, using the precipitation procedures described above. The regenerated electrolyte was fed into an assembled cell at 20 °C from two syringe pumps at the flow rates of 0.025, 0.037, 0.037 mL/min for 100, 150, 200 mA/cm^2 respectively. These current densities and flow rates correspond to 2.5, 2.5, and 3.3 M nominal production of acid and base, respectively. After performing the standard break-in procedure described above, the cell was set to pass a specified current with a 2 minute current reversal every 5 hours (for a 99.3% duty cycle). We have previously found that these periodic current reversals are necessary for maintaining the GDE's voltage stability and to dissolve any hydroxide precipitates that may accumulate on the cathode [47, 48]. When the syringe pumps were low on electrolyte, the potentiostat was briefly paused (< 4 mins) to refill them. During the re-filling process, a small amount of bubbles were seen passing through the anolyte and catholyte outlet lines as the pumps were restarted, which were likely stuck on the polypropylene spacer despite its plasma treatment. The liberation of these small bubbles explains the slight improvement in voltage observed after each re-filling.

Supporting Information

Supporting Information document contains the following: Supporting Notes regarding reaction stoichiometry, alkaline error; Supporting Figures on pH changes, LSVs of DFC, charge transport in the DFC by species identity, picture of hydrogen peroxide decomposition, pH change during Li_2CO_3 precipitation, pXRD of variously washed Li_2CO_3, photos of leachate precipitates, GEIS data for the DFC; Supporting Tables for DFC performance metrics, DFC output speciation and pH, elemental analysis of transition metal hydroxides, residual concentration of transition metals, data for Fig. 5b, preliminary input cost analysis

Statements and Declarations

Competing Interests

A PCT patent application has been filed which covers some elements of this work. The authors are inventors on the patent.

Funding

Support for this research is provided by the Precourt Institute for Energy and SLAC-Stanford Battery Center seed grant, the Canadian Institute for Advanced Research, and the Precourt Institute for Energy Chevron Energy Fellows Program. JWM is supported by a National Science Foundation Graduate Research Fellowship and BPC is supported by a fellowship from the Stanford Center for Molecular Analysis and Design.

Acknowledgements

Part of this work was performed at nano@stanford RRID:SCR_026695. Dr. Guangchao Li contributed to the collection of ICP-OES data

Author Contributions

Conceptualization: JWM, JGW, BPC, MWK. Methodology: JWM. Investigation: JWM. Formal Analysis: JWM. Visualization: JWM. Funding Acquisition: MWK. Project Administration: MWK. Supervision: MWK. Writing- original draft: JWM. Writing- review and editing: JWM, JGW, BPC, MWK.

Data Availability

Data supporting this study is available in the Main Text and Supporting Information. Data for Figure 2 is available in Supporting Tables S1 and S2. Data for Figure 5 is available in Supporting Table S8. Additional data is available on reasonable to the corresponding author.

References:

1. (2025) Electric vehicle batteries – Global EV Outlook 2025 – Analysis. International Energy Agency https://www.iea.org/reports/global-ev-outlook-2025/electric-vehicle-batteries. Accessed 19 November 2025

2. Bernhart W, Heimes H, Kampker A (2025) Battery Monitor 2024/2025. Roland Berger GmbH: Munich, Germany. https://www.rolandberger.com/en/Insights/Publications/Battery-Monitor-2024-2025-A-turbulent-year-and-outlook-for-value-chain-players.html. Accessed 15 November 2025

3. (2025) Electric Vehicle Outlook 2025. BloombergNEF, London, UK. https://about.bnef.com/insights/clean-transport/electric-vehicle-outlook/. Accessed 15 November 2025

4. (2025) Market and Innovation Trends in Battery Recycling. CAS & Deloitte. https://www.cas.org/resources/cas-insights/lithium-ion-battery-recycling-trends. Accessed 17 November 2025

5. Fleischmann J, Hanicke M, Horetsky E, Ibrahim D, Sören J, Linder M, Schaufuss P, Torscht LT, van de Rijt A (2023) Battery 2030: Resilient, Sustainable, and Circular.

Global Battery Alliance & McKinsey & Co. https://www.globalbattery.org/publications/battery-2030-resilient,-sustainable,-and-circular/. Accessed 09 September 2025

6. (2021) National Blueprint for Lithium Batteries 2021-2030. Federal Consortium for Advanced Batteries. https://www.energy.gov/eere/vehicles/articles/national-blueprint-lithium-batteries. Accessed 20 November 2025

7. European Commission, Brussels (2023) Regulation (EU) 2023/1542 of the European Parliament and of the Council of 12 July 2023 concerning batteries and waste batteries, amending Directive 2008/98/EC and Regulation (EU) 2019/1020 and repealing Directive 2006/66/EC. https://eur-lex.europa.eu/eli/reg/2023/1542/oj/eng. Accessed 10 October 2025

8. Marie J-J, Gifford S (2025) Insight 18: Developments in Lithium-Ion Battery Cathodes. The Faraday Institution, Oxford, England. https://www.faraday.ac.uk/insights/insight-18-developments-in-lithium-ion-battery-cathodes/. Accessed 20 November 2025

9. Gaines L, Zhang J, He X, Bouchard J, Melin HE (2023) Tracking Flows of End-of-Life Battery Materials and Manufacturing Scrap. Batteries 9:360. https://doi.org/10.3390/batteries9070360

10. Rostami H, Valio J, Tynjälä P, Lassi U, Suominen P (2024) Life Cycle of LiFePO4 Batteries: Production, Recycling, and Market Trends. ChemPhysChem 25:e202400459. https://doi.org/10.1002/cphc.202400459

11. Davis K, Demopoulos GP (2023) Hydrometallurgical recycling technologies for NMC Li-ion battery cathodes: current industrial practice and new R&D trends. RSC Sustain 1:1932–1951. https://doi.org/10.1039/D3SU00142C

12. An L (ed.) (2019) Recycling of Spent Lithium-Ion Batteries: Processing Methods and Environmental Impacts. Springer International Publishing, Cham

13. Rezaei M, Nekahi A, Kumar M R A, Nizami A, Li X, Deng S, Nanda J, Zaghib K (2025) A review of lithium-ion battery recycling for enabling a circular economy. J Power Sources 630:236157. https://doi.org/10.1016/j.jpowsour.2024.236157

14. Kim C-H, Kim M-J, Jeon K-W, Jeon I-J, Yoon C-M, Gong J-H, Yoon E-S, Lim J-H, Roh H-S, Chae S, Jang W-J, Shim J-O (2025) Advancing sustainable treatment of sodium sulfate (Na2SO4)-containing wastewater: Recent advances in electrochemical technologies. Chem Eng J 524:169100. https://doi.org/10.1016/j.cej.2025.169100

15. Bernhart W, Kampker A, Heimes H (2022) Battery Monitor 2022. Roland Berger GmbH: Munich, Germany. https://www.rolandberger.com/en/Insights/Publications/Battery-Monitor-2022-

Technology-and-sustainability-in-the-battery-market.html. Accessed 20 November 2025

16. Peeters N, Binnemans K, Riaño S (2020) Solvometallurgical recovery of cobalt from lithium-ion battery cathode materials using deep-eutectic solvents. Green Chem 22:4210–4221. https://doi.org/10.1039/D0GC00940G

17. Aannir M, Hakkou R, Levard C, Taha Y, Ghennioui A, Rose J, Saadoune I (2023) Towards a closed loop recycling process of end-of-life lithium-ion batteries: Recovery of critical metals and electrochemical performance evaluation of a regenerated LiCoO2. J Power Sources 580:233341. https://doi.org/10.1016/j.jpowsour.2023.233341

18. Han B, Anwar UI Haq R, Louhi-Kultanen M (2020) Lithium carbonate precipitation by homogeneous and heterogeneous reactive crystallization. Hydrometallurgy 195:105386. https://doi.org/10.1016/j.hydromet.2020.105386

19. Battaglia G, Berkemeyer L, Cipollina A, Cortina JL, Fernandez de Labastida M, Lopez Rodriguez J, Winter D (2022) Recovery of Lithium Carbonate from Dilute Li-Rich Brine via Homogenous and Heterogeneous Precipitation. Ind Eng Chem Res 61:13589–13602. https://doi.org/10.1021/acs.iecr.2c01397

20. Li L, Dunn JB, Zhang XX, Gaines L, Chen RJ, Wu F, Amine K (2013) Recovery of metals from spent lithium-ion batteries with organic acids as leaching reagents and environmental assessment. J Power Sources 233:180–189. https://doi.org/10.1016/j.jpowsour.2012.12.089

21. Henderson MS, Beh CC, Oraby E, Eksteen J (2025) Organic Acid Leaching of Black Mass with an LFP and NMC Mixed Chemistry. Recycling 10:145. https://doi.org/10.3390/recycling10040145

22. Gerold E, Schinnerl C, Antrekowitsch H (2022) Critical Evaluation of the Potential of Organic Acids for the Environmentally Friendly Recycling of Spent Lithium-Ion Batteries. Recycling 7:4. https://doi.org/10.3390/recycling7010004

23. Gao W, Zhang X, Zheng X, Lin X, Cao H, Zhang Y, Sun Z (2017) Lithium Carbonate Recovery from Cathode Scrap of Spent Lithium-Ion Battery: A Closed-Loop Process. Environ Sci Technol 51:1662–1669. https://doi.org/10.1021/acs.est.6b03320

24. Yu M, Zhang Z, Xue F, Yang B, Guo G, Qiu J (2019) A more simple and efficient process for recovery of cobalt and lithium from spent lithium-ion batteries with citric acid. Sep Purif Technol 215:398–402. https://doi.org/10.1016/j.seppur.2019.01.027

25. Li L, Ge J, Chen R, Wu F, Chen S, Zhang X (2010) Environmental friendly leaching reagent for cobalt and lithium recovery from spent lithium-ion batteries. Waste Manag 30:2615–2621. https://doi.org/10.1016/j.wasman.2010.08.008

26. Yang T, Luo D, Zhang X, Gao S, Gao R, Ma Q, Park HW, Or T, Zhang Y, Chen Z (2024) Sustainable regeneration of spent cathodes for lithium-ion and post-lithium-ion batteries. Nat Sustain 1–10. https://doi.org/10.1038/s41893-024-01351-5

27. Iturrondobeitia M, Vallejo C, Berroci M, Akizu-Gardoki O, Minguez R, Lizundia E (2022) Environmental Impact Assessment of LiNi1/3Mn1/3Co1/3O2 Hydrometallurgical Cathode Recycling from Spent Lithium-Ion Batteries. ACS Sustain Chem Eng 10:9798–9810. https://doi.org/10.1021/acssuschemeng.2c01496

28. Lv W, Wang Z, Cao H, Sun Y, Zhang Y, Sun Z (2018) A Critical Review and Analysis on the Recycling of Spent Lithium-Ion Batteries. ACS Sustain Chem Eng 6:1504–1521. https://doi.org/10.1021/acssuschemeng.7b03811

29. Kumar Vinayak A, Majid M, Xia L, Wang X (2025) Critical Review of Acid Leaching for Recovery of Valuable Metals from Spent Lithium-ion Batteries. Electrochem Energy Rev 8:25. https://doi.org/10.1007/s41918-025-00266-9

30. Li L, Bian Y, Zhang X, Xue Q, Fan E, Wu F, Chen R (2018) Economical recycling process for spent lithium-ion batteries and macro- and micro-scale mechanistic study. J Power Sources 377:70–79. https://doi.org/10.1016/j.jpowsour.2017.12.006

31. Wang J-Z, Tang Y-C, Shen Y-H (2025) Optimizing Organic Acid Leaching of Spent Lithium-Ion Batteries Using Material Flow Cost Accounting (MFCA). Processes 14:. https://doi.org/10.3390/pr14010023

32. Fang Z, Zhu P, Zhang X, Feng Y, Wang H (2025) Self-looped electrochemical recycling of lithium-ion battery cathode materials to manufacturing feedstocks. Nat Chem Eng 2:142–151. https://doi.org/10.1038/s44286-025-00186-x

33. Asadi A, Kang D, Bazargan Harandi H, Chung-Yen Jung J, Sui P-C (2024) Utilization of lithium sulphate electrodialysis for closed-loop LIB recycling: Experimental study and process simulation. Sep Purif Technol 343:126989. https://doi.org/10.1016/j.seppur.2024.126989

34. Zhu J, Asadi A, Kang D, Chung-Yen Jung J, Abel Chuang P-Y, Sui P-C (2025) Bipolar membranes electrodialysis of lithium sulfate solutions from hydrometallurgical recycling of spent lithium-ion batteries. Sep Purif Technol 354:128715. https://doi.org/10.1016/j.seppur.2024.128715

35. Cerrillo-Gonzalez MM, Villen-Guzman M, Vereda-Alonso C, Gomez-Lahoz C, Rodriguez-Maroto JM, Paz-Garcia JM (2020) Recovery of Li and Co from LiCoO2 via Hydrometallurgical–Electrodialytic Treatment. Appl Sci 10:2367. https://doi.org/10.3390/app10072367

36. Jung JC-Y, Chow N, Nacu A, Melashvili M, Cao A, Khorbaladze L, Meseldzija Z, Sui JP-C, Zhang J (2021) A Novel Closed Loop Process For Recycling Spent Li-Ion

Battery Cathode Materials. Int J Green Energy 18:1597–1612. https://doi.org/10.1080/15435075.2021.1914631

37. Kim J, Moon I, Kim J (2023) Integration of wastewater electro-electrodialysis and CO2 capture for sustainable LIB recycling: Process design and economic analyses. J Clean Prod 391:136241. https://doi.org/10.1016/j.jclepro.2023.136241

38. Isaksson A, Anaya Garzon J, Strandkvist I, Öqvist LS (2025) Zero-waste recycling of lithium and cobalt from lithium-ion batteries by three-stage electrodialysis. Sep Purif Technol 368:133060. https://doi.org/10.1016/j.seppur.2025.133060

39. Luc W, Schroeter HV, Voigt P (2024) Electrochemical production of alkali metal hydroxides and sulfuric acid from battery manufacturing and recycling outlet streams. WO2024064916A2, March 28, 2024.

40. Fang J, Ding Z, Ling Y, Li J, Zhuge X, Luo Z, Ren Y, Luo K (2022) Green recycling and regeneration of LiNi0.5Co0.2Mn0.3O2 from spent Lithium-ion batteries assisted by sodium sulfate electrolysis. Chem Eng J 440:135880. https://doi.org/10.1016/j.cej.2022.135880

41. Ding Z, Li J, Huang Y, Lin H, Wei P, Li J, Zhuge X, Yang Z, Qu K, Ren Y (2025) Closing the Loop on Lithium-Ion Battery Cathodes: A Green Electrometallurgical Recycling Approach. ACS Sustain Chem Eng 13:1570–1581. https://doi.org/10.1021/acssuschemeng.4c07920

42. O'Brien TF, Bommaraju TV, Hine F (2005) Brine Preparation and Treatment. In: Handbook of Chlor-Alkali Technology: Volume I: Fundamentals, Volume II: Brine Treatment and Cell Operation, Volume III: Facility Design and Product Handling, Volume IV: Plant Commissioning and Support Systems, Volume V: Corrosion, Environmental Issues, and Future Development. Springer US, Boston, MA, pp 465–703

43. Wang Q, Yang P, Cong W (2011) Cation-exchange membrane fouling and cleaning in bipolar membrane electrodialysis of industrial glutamate production wastewater. Sep Purif Technol 79:103–113. https://doi.org/10.1016/j.seppur.2011.03.024

44. Reig M, Casas S, Gibert O, Valderrama C, Cortina JL (2016) Integration of nanofiltration and bipolar electrodialysis for valorization of seawater desalination brines: Production of drinking and waste water treatment chemicals. Desalination 382:13–20. https://doi.org/10.1016/j.desal.2015.12.013

45. Mikhaylin S, Bazinet L (2016) Fouling on ion-exchange membranes: Classification, characterization and strategies of prevention and control. Adv Colloid Interface Sci 229:34–56. https://doi.org/10.1016/j.cis.2015.12.006

46. Thiel GP, Kumar A, Gómez-González A, Lienhard JHV (2017) Utilization of Desalination Brine for Sodium Hydroxide Production: Technologies, Engineering

Principles, Recovery Limits, and Future Directions. ACS Sustain Chem Eng 5:11147–11162. https://doi.org/10.1021/acssuschemeng.7b02276

47. Charnay BP, Chen Y, Misleh JW, Wright JG, Agarwal RG, Sauvé ER, Toh WL, Surendranath Y, Kanan MW (2025) Membrane-free electrochemical production of acid and base solutions capable of processing ultramafic rocks. Nat Commun 16:9759. https://doi.org/10.1038/s41467-025-64595-5

48. Wright JG, Kanan MW (2025) Electrochemical Production of >1 M Acid and Base from Neutral Salt at High Current Density and Low Energy Demand. ACS Energy Lett 5328–5335. https://doi.org/10.1021/acsenergylett.5c02318

49. Corti H, Crovetto R, Fernández-Prini R (1979) Aqueous solutions of lithium hydroxide at various temperatures: Conductivity and activity coefficients. J Solut Chem 8:897–908. https://doi.org/10.1007/BF00644886

50. Baes CFJr (1957) The Estimation of Bisulfate Ion Dissociation in Sulfuric Acid-Sodium Sulfate Solutions. J Am Chem Soc 79:5611–5616. https://doi.org/10.1021/ja01578a008

51. Elgquist B, Wedborg M (1974) Sulphate complexation in seawater: A relation between the stability constants of sodium sulphate and magnesium sulphate in seawater from a determination of the stability constant of hydrogen sulphate and a calculation of the single ion activity coefficient of sulphate. Mar Chem 2:1–15. https://doi.org/10.1016/0304-4203(74)90002-4

52. Billy E, Joulié M, Laucournet R, Boulineau A, De Vito E, Meyer D (2018) Dissolution Mechanisms of LiNi1/3Mn1/3Co1/3O2 Positive Electrode Material from Lithium-Ion Batteries in Acid Solution. ACS Appl Mater Interfaces 10:16424–16435. https://doi.org/10.1021/acsami.8b01352

53. Cerrillo-Gonzalez M del M, Villen-Guzman M, Acedo-Bueno LF, Rodriguez-Maroto JM, Paz-Garcia JM (2020) Hydrometallurgical Extraction of Li and Co from LiCoO2 Particles–Experimental and Modeling. Appl Sci 10:6375. https://doi.org/10.3390/app10186375

54. Cerrillo-Gonzalez MM, Villen-Guzman M, Vereda-Alonso C, Rodriguez-Maroto JM, Paz-Garcia JM (2022) Acid leaching of LiCoO2 enhanced by reducing agent. Model formulation and validation. Chemosphere 287:132020. https://doi.org/10.1016/j.chemosphere.2021.132020

55. Vetter TA, Colombo DPJr (2003) Kinetics of Platinum-Catalyzed Decomposition of Hydrogen Peroxide. J Chem Educ 80:788. https://doi.org/10.1021/ed080p788

56. Bommel A van, Dahn JR (2009) Synthesis of Spherical and Dense Particles of the Pure Hydroxide Phase Ni1／3Mn1／3Co1／3 (OH) 2. J Electrochem Soc 156:A362. https://doi.org/10.1149/1.3079366

57. Yabuuchi N, Koyama Y, Nakayama N, Ohzuku T (2005) Solid-State Chemistry and Electrochemistry of LiCo1／3Ni1／3Mn1／3O2 for Advanced Lithium-Ion Batteries: II. Preparation and Characterization. J Electrochem Soc 152:A1434. https://doi.org/10.1149/1.1924227

58. Chan KH, Anawati J, Malik M, Azimi G (2021) Closed-Loop Recycling of Lithium, Cobalt, Nickel, and Manganese from Waste Lithium-Ion Batteries of Electric Vehicles. ACS Sustain Chem Eng 9:4398–4410. https://doi.org/10.1021/acssuschemeng.0c06869

59. Wang H, Friedrich B (2015) Development of a Highly Efficient Hydrometallurgical Recycling Process for Automotive Li–Ion Batteries. J Sustain Metall 1:168–178. https://doi.org/10.1007/s40831-015-0016-6

60. Chernyaev A, Zhang J, Seisko S, Louhi-Kultanen M, Lundström M (2023) Fe3+ and Al3+ removal by phosphate and hydroxide precipitation from synthetic NMC Li-ion battery leach solution. Sci Rep 13:21445. https://doi.org/10.1038/s41598-023-48247-6

61. Chen X, Ruan X, Kentish SE, Li G (Kevin), Xu T, Chen GQ (2021) Production of lithium hydroxide by electrodialysis with bipolar membranes. Sep Purif Technol 274:119026. https://doi.org/10.1016/j.seppur.2021.119026

62. Hou B, Fu R, Wang H, Yan J, Li R, Wang B, Jiang C, Wang Y, Xu T (2023) One-step conversion of sulfate lithium into high-purity lithium hydroxide crystals via bipolar membrane crystallization. AIChE J 69:e18208. https://doi.org/10.1002/aic.18208

63. Nemkov NM, Ryabtsev AD, Kotsupalo NP (2020) Preparing High-Purity Lithium Hydroxide Monohydrate by the Electrochemical Conversion of Highly Soluble Lithium Salts. Theor Found Chem Eng 54:710–718. https://doi.org/10.1134/S0040579519050166